



OPEN

Analysis of rainfall response and graded warning for landslides

Yin Xing^{1,2✉}, Peng Wang¹ & Saipeng Huang³

Rainfall-induced landslides are characterized by stochasticity and complexity, making the development of effective early warning models crucial for disaster prevention and mitigation. Focusing on creeping landslides in Zigui County within the Three Gorges Reservoir area, this study proposes a rainfall early warning method based on a displacement ratio model. By analyzing the response relationship between landslide displacement and cumulative rainfall, a time-phased exponential early warning model was established, along with four-level warning thresholds (78.3 mm, 160.1 mm, and 196.6 mm). The model, which uses cumulative rainfall as the core input variable, explains approximately 30–40% of the variation in landslide displacement. Validation using three landslide events in 2021 and historical extreme rainfall events shows that the model successfully issued warnings for all incidents (100% recall), albeit with an 8% false alarm rate. The proposed method features concise parameters and strong operability, offering a technical reference for landslide early warning in similar regions, though its applicability should be further validated in conjunction with specific geological conditions.

Keywords Three Gorges reservoir area, Creeping landslides, Rainfall warning, Monitoring

Landslides are among the most destructive geological hazards, causing significant economic losses and casualties¹. Rainfall is the most common trigger of landslide destabilization². Therefore, identifying triggering factors, predicting landslide stability, and establishing accurate early warning models are essential for avoiding major losses. At present, the early warning and forecasting studies of rainfall-type landslides are mainly of the following types³: (1) deterministic methods based on physical and hydrological models, which use generalized models to study landslide deformation laws to provide a basis for landslide prediction and forecasting. Such methods need to obtain the parameters of the geotechnical body, and it is difficult to quantify the impact of rainfall induced landslides due to the variability of geological conditions and geological environment, and the complexity of the change process of the geotechnical parameters during rainfall; (2) establishing empirical rainfall thresholds by establishing the relationship between landslide events and cumulative rainfall^{4–6}. However, these empirical thresholds are influenced by rainfall patterns, the choice of rainfall intensity-duration combinations, and regional differences in geological and climatic conditions. As a result, thresholds developed for one area may not be directly transferable to other regions, leading to poor predictive accuracy for rainfall-induced landslides⁷. problems, resulting in poor objective accuracy in the selection of rainfall thresholds for induced landslides; (3) based on certain deterministic models to predict the destabilization time of landslides^{8–11}. Since this type of model presupposes that the deformation time relationship satisfies a particular model, it is difficult to express the characteristics of uncertainty and sudden change that exist in the actual landslide evolution. Therefore, the prediction accuracy is relatively limited. Due to the complexity and variability of the geological environment, influencing factors, and disaster-causing mechanisms of landslides, it is difficult to accurately describe the trend of landslide disaster-causing and provide reasonable warning information by relying on a single warning indicator. Considering the significance of engineering practice and disaster warning, the early warning of landslides should focus on the research and modeling of short term and disaster warning criteria. Therefore, it is of great significance to establish an early warning system by analyzing the deformation monitoring data of step type landslides. In this study, “creeping landslides” refer to landslides characterized by slow, continuous deformation without overall failure. These landslides typically exhibit low displacement rates (mm to cm per year) and step-like displacement–time curves. Under external triggers such as heavy rainfall, they may experience brief accelerated deformation but do not immediately undergo catastrophic sliding.

It is noteworthy that existing rainfall early warning studies have predominantly focused on real-time warnings for critical sliding events^{12–15}, while paying insufficient attention to the brief accelerated deformation phase

¹School of Geography Science and Geomatics Engineering, Suzhou University of Science and Technology, Suzhou 215009, China. ²Research Center of Water Engineering Safety and Disaster Prevention of Ministry of Water Resources, Wuhan 430010, China. ³School of Resources and Safety Engineering, Chongqing University, Chongqing 400030, China. ✉email: yxin0320@163.com

of creeping landslides following heavy rainfall. Although these landslides exhibit overall slow movement, the accelerated deformation still poses a serious threat to the safety of residents' lives and property on the landslide mass. Furthermore, the statistical variables used in existing studies are often the number of landslides or absolute displacement values, without adequately considering the influence of the landslides' scale characteristics^{16–20}. To address these issues, this study takes creeping landslides in Zigui County, Three Gorges Reservoir area, as an example and proposes a practical rainfall warning model with concise parameters and easy operability. The core research approach is as follows: (1) introducing the displacement ratio (displacement/landslide length) as a deformation indicator to eliminate the influence of scale; (2) focusing on cumulative rainfall as the main controlling factor to simplify model inputs; (3) establishing a time-phased exponential model to determine graded warning thresholds. This model aims to achieve graded warnings for creeping landslides using a single key variable, providing a scientific basis for decision-making by management authorities.

Materials and methods

Natural environmental conditions in the study area

Zigui County (2427 km²) is located on both banks of the Yangtze River's Xiling Gorge in Yichang City, western Hubei Province. The Yangtze River bisects the county from west to east, creating a basin landscape with higher terrain on the north bank and lower terrain on the south bank, and vice versa on the south bank (Fig. 1). The river flows approximately 247.8 km through the county, with a watershed area of 1952.5 km². Zigui County's climate is classified as subtropical monsoon, with a lot of rainfall and an average yearly temperature between 17 and 19 °C, based on meteorological data. The average annual rainfall in Zigui County has been 1493.2 mm for a number of years. The average monthly rainfall is 150–457.6 mm. From April to October, there is a more concentrated concentration of rainfall, with daily totals of up to 50–100 mm. From June to July, the rainy season begins, and there are likely three–four times as many rainstorms as there have been extremely heavy rainfall up to this point. Zigui County is a part of the Yangtze River flow. The Yangtze River passes through Zigui County, and the county has a sophisticated water system with interconnected rivers, an abundance of water resources, and water levels that increase and decrease by up to 30 m.

Overview of landslides in the study area

Zigui County has a diverse and well-developed stratigraphy, with exposed strata ranging from the Yuan Gu Jie to the Quaternary. The topography and geological structure of the area are complex, and the mountain body has led to increased alluvial gully development. Zigui County has a warm, humid subtropical monsoon climate with

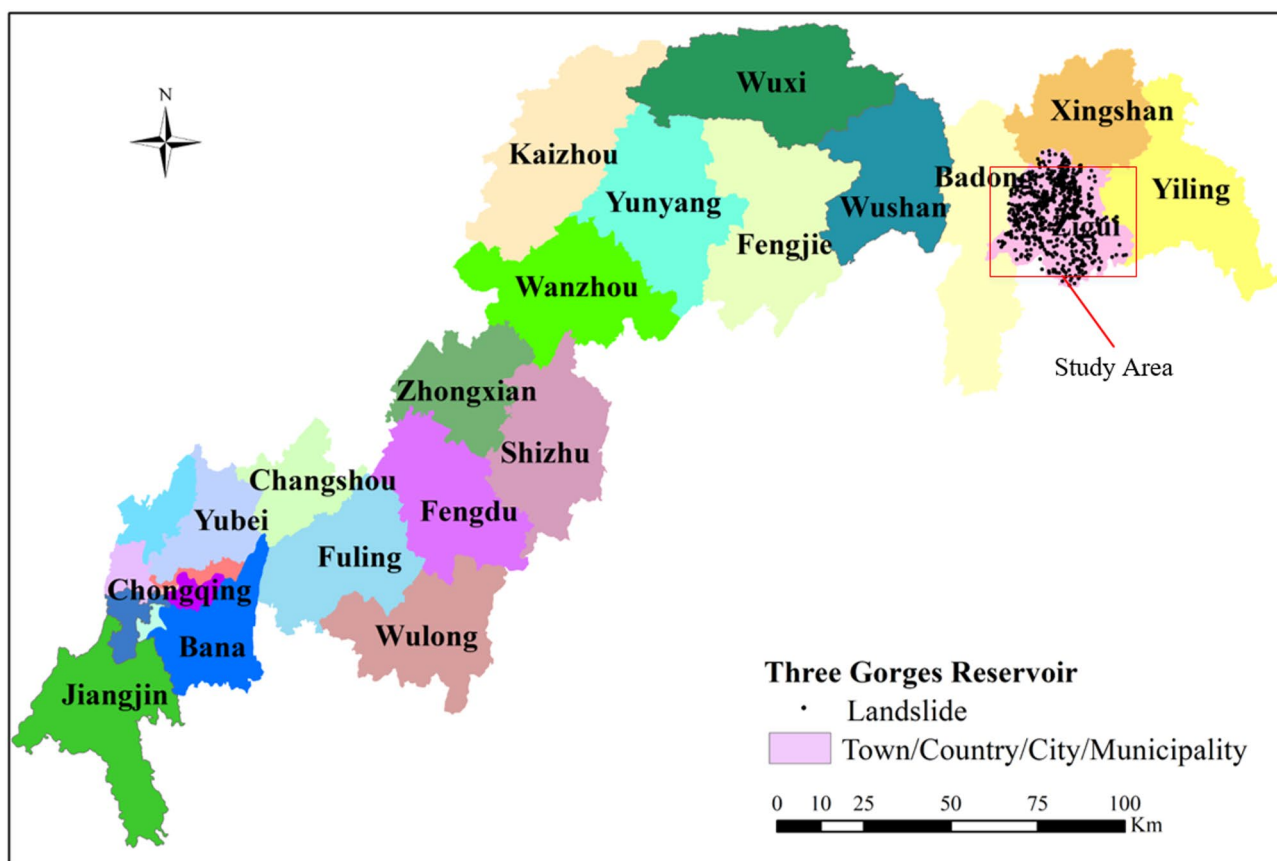


Fig. 1. The location of Zigui and distribution of the landslides.

plenty of rainfall, mountains, trees, and lush vegetation. The rainy season is marked by recurrent episodes of heavy, prolonged, and continuous rain as well as other wet weather conditions. One of the factors contributing to the high frequency of landslides in Zigui County is its unique climate and geomorphological circumstances. Landslides are a form of geological hazard that are considered to be the most significant in Zigui County because they are a result of the wide-spread, dangerous, group occurrence of higher law²¹⁻²³. Three primary factors led to the district's selection: (1) From 2016 to 2018, a geological survey project was carried out in the region. As a result, there is a comparatively comprehensive inventory of landslides, which is crucial for determining the sensitivity of landslides. (2) There are several different kinds of landslides in the region, and taking these into account makes landslide sensitivity studies easier. Furthermore, the area's moderate landslide density and number in comparison to some other research²⁴ offers enough landslide sample points for statistically based modeling. (3) The modest complexity of the geological environment permits the proper amount of complexity of the input data (number of intervals, for example) to be maintained.

Figure 2 presents a flowchart summarizing the overall methodology of this study, which consists of four main stages: (1) data collection and screening, (2) determination of rainfall statistical variables and landslide deformation indicators, (3) establishment of the rainfall threshold model and warning system, and (4) model validation.

Establishment of rainfall warning model Examining samples of data from displacement monitoring

The real landslide displacement cumulative curve will appear to increase, missing amplitude and other anomalies, and will present complex and diverse characteristics due to the monitoring method, formation mechanism, measurement errors, and other factors on the landslide in the actual engineering. As a result, various landslide displacement accumulation curves represent the various landslide features.

Based on cumulative displacement curve characteristics (Fig. 3), landslides in Zigui County can be classified into six types²⁵:

Smooth type: Stable deformation with linear cumulative displacement.

Uniform type: Constant deformation rate, indicating either initial or steady-state creep.

Convergent type: Initial accelerated deformation followed by deceleration due to protective measures or reduced external forces.

Accelerating type: Increasing displacement rate leading to eventual failure.

Fall-back type: Temporary displacement decrease due to crack closure under pressure.

Step-type: Alternating slow and accelerated deformation in response to periodic triggers like rainfall and reservoir fluctuations (e.g., Sifangbei landslide).

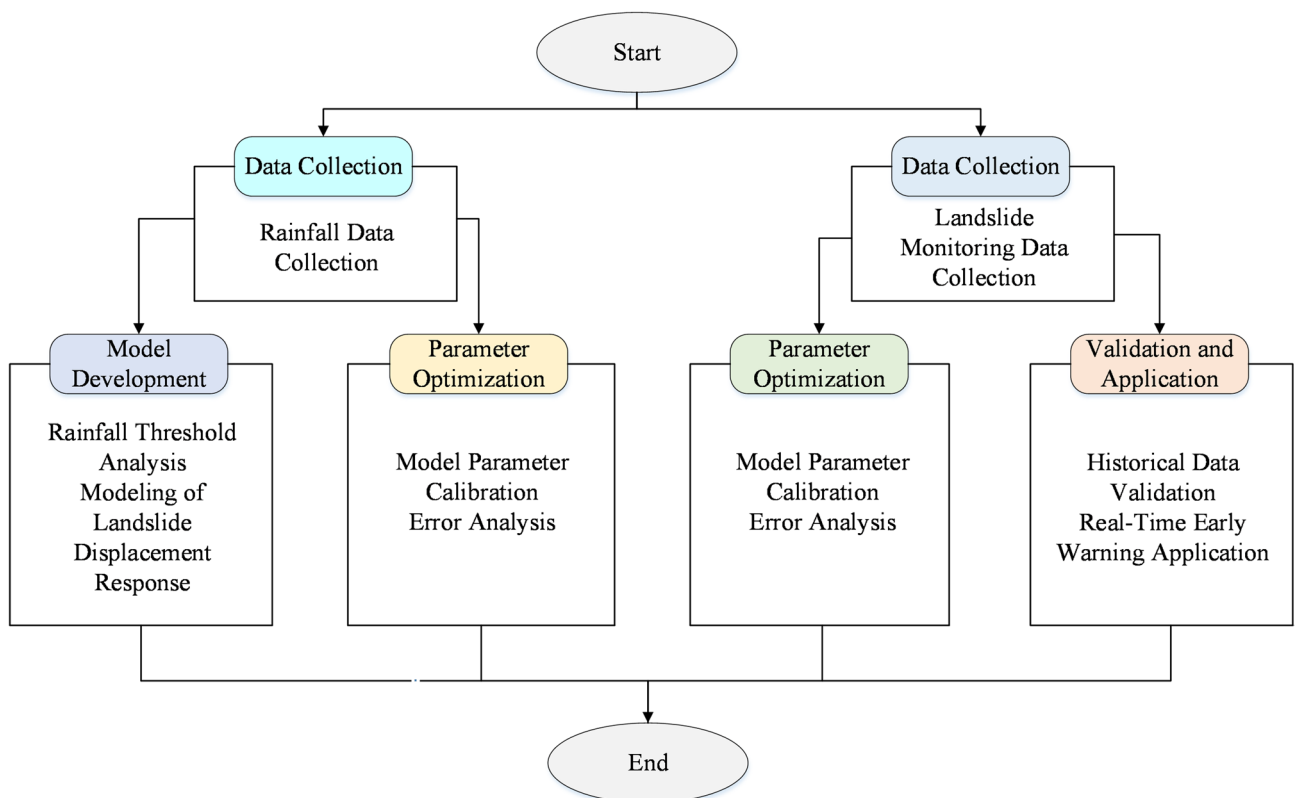


Fig. 2. Technical flowchart.

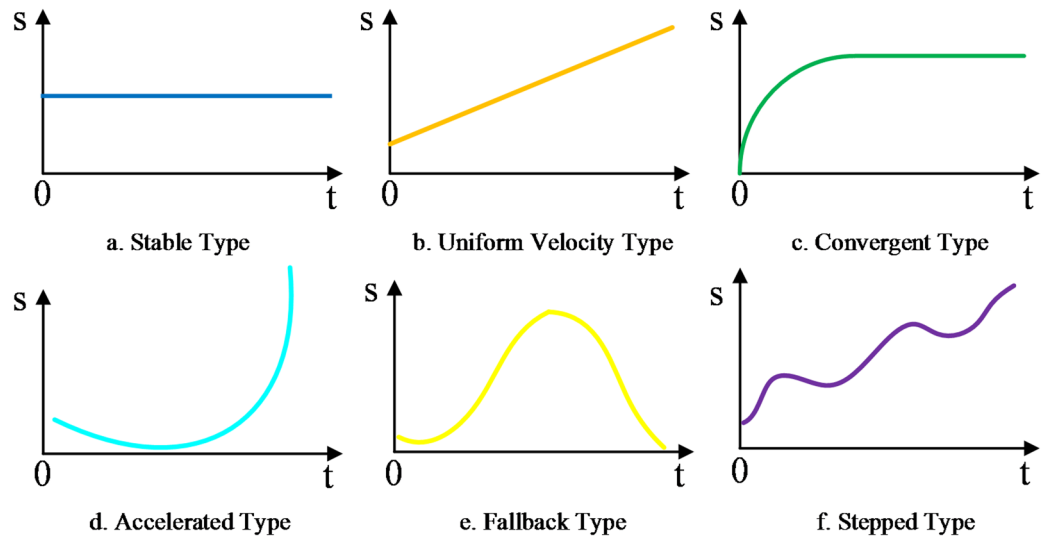


Fig. 3. Different kinds of cumulative displacement curves of landslide.

Among these, step-type landslides are the focus of this study, as they are most sensitive to rainfall and exhibit clear deformation responses.

Multiple GPS monitoring sites, arranged as one to three monitoring profiles, are placed on each landslide in the research area's current monitoring system. The landslide monitoring data is compared and analyzed, and it is discovered that all six of the aforementioned displacement profiles occur. At various GPS monitoring stations within the same landslide, distinct displacement curves may occasionally emerge as a result of unintentional mistakes or spatial inhomogeneity of landslide deformation. Nevertheless, landslide movement during or after rainfall is given more consideration in the development of landslide rainfall warning models, and it is meaningless to include landslide displacement data in statistical samples if there isn't a clear indication of accelerated deformation (smooth curve). Thus, to eliminate the impact of both uneven deformation within the landslide itself and interference from landslides in a stable state, a statistical sample was formed by first selecting 3–4 groups of GPS monitoring point data with similar deformation characteristics from each landslide. The screening criteria were as follows: (1) the deformation trend of the GPS monitoring point was more evident in recent years; and (2) the selected GPS monitoring points on the same landslide were in the same monitoring profile of that landslide or could form a strong deformation zone. Following a statistical analysis of each monitoring point's displacement components along the main slide direction, the monitoring points whose average annual displacement components along the main slide direction were less than 10 mm over the course of the monitoring period were excluded due to the systematic error of the GPS equipment.

Determination of rainfall statistics variables

Dividing the duration of the study

Only the reservoir water level variable may be reasonably controlled to evaluate the effect of rainfall on landslides independently. Rainfall and fluctuations in reservoir water levels are key factors determining landslide movement in reservoir locations^{26,27}. In order to maintain a constant reservoir water level over time, it is required to split the time period suitably. Following this, a statistical analysis of the rainfall during each time period must be conducted.

Reservoir water level fluctuation is another important factor influencing landslides in the reservoir area. To minimize its interference as much as possible and focus on the effects of rainfall, this study divided the analysis period into three stages based on the flood season operation mode of the Three Gorges Reservoir: May, June–August, and September. Historical data show that only 11.5% of landslides occurred from October to April of the following year^{28–33}, indicating that periods of slow water level rise and decline have a limited impact on landslide stability (Fig. 4). This finding validates the rationality of the study period division in this research.

Calculating rainfall parameters

In general, periods of excessive rainfall, such as the longest continuous rainfall, the largest single day rainfall, and the cumulative rainfall over several days, are when landslides typically occur³⁴. A correlation analysis was conducted using Matlab software to find the correlation coefficients between various rainfall factors and the occurrence of landslides. Pearson correlation coefficients were calculated for cumulative rainfall over n consecutive days ($n = 1$ to 10) based on 36 landslide events recorded in the study area between 2010 and 2020, together with daily rainfall data from the Yichang meteorological station. The findings indicate that, although the value of n varies over time, the cumulative rainfall over a period of n consecutive days is most significant in predicting landslide occurrence. For each period, the n value with the highest correlation coefficient and statistical significance ($p < 0.05$) was selected. When multiple n values showed similar correlations, the frequency of the corresponding rainfall processes in the study area was considered to ensure sufficient sample size for

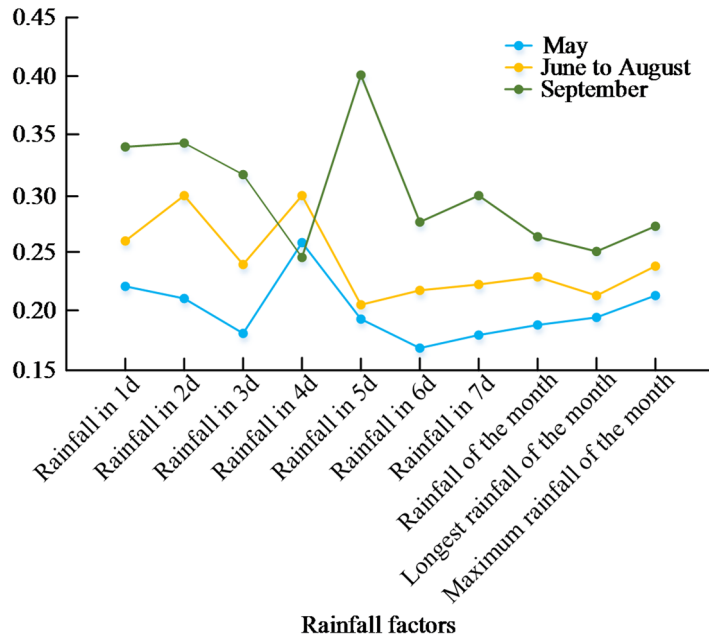


Fig. 4. The correlation relationship between rainfall index and landslide in n days before landslide.

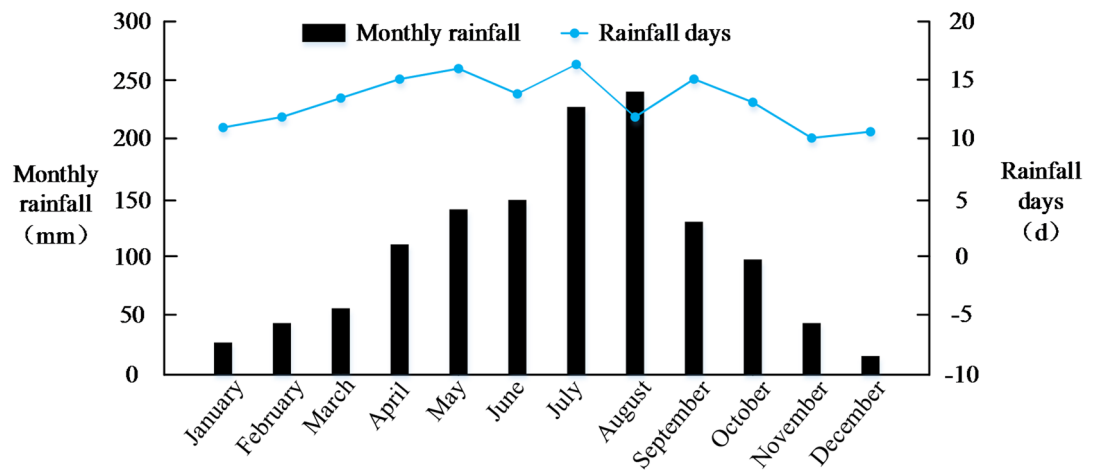


Fig. 5. The duration distribution of rainfall process in the rainy season in Zigui.

subsequent analysis. Since the cumulative rainfall on the fourth day prior to a landslide in May has a much higher correlation coefficient than other components, n is set at 4. In a similar vein, the cumulative rainfall on the fifth day prior to the landslide, that is, n = 5, has the strongest link with the landslide from June to August. The correlation coefficients are highest in September at n = 2 and n = 4. The distribution of rainfall durations during the flood season was further counted, and it was discovered that (Fig. 5) that the cumulative rainfall events of four consecutive days in September at Zigui County were significantly greater than the cumulative events of two consecutive days. In September, therefore, n was taken as 4 to guarantee the number of available statistical samples.

The optimal number of consecutive days n for each period was determined by maximizing the Pearson correlation coefficient:

$$n_{opt} = \arg \max_{n \in [1,10]} |r_n| \tag{1}$$

where r_n is the correlation coefficient between cumulative rainfall over n consecutive days and landslide occurrence, calculated as:

$$r_n = \frac{\sum_{i=1}^N (R_{n,i} - \bar{R}_n)(L_i - \bar{L})}{\sqrt{\sum_{i=1}^N (R_{n,i} - \bar{R}_n)^2 \sum_{i=1}^N (L_i - \bar{L})^2}} \quad (2)$$

where $R_{n,i}$ is the cumulative rainfall over n days prior to the i -th landslide event, \bar{R}_n is the mean of $R_{n,i}$, L_i is a binary indicator of landslide occurrence (1 for event days, 0 for non-event days), and \bar{L} is the mean of L_i . Only days with valid rainfall records were included in the analysis.

In general, the amount of rainfall that causes a landslide to deform is positively correlated with the amount of rainfall; however, only rainfall processes that exceed a certain amount can cause landslides to begin moving³⁵. Additionally, statistical efficiency will be decreased if all rainfall events are statistically analyzed. Determining the minimum amount of rainfall required in the area to cause landslides is therefore essential. First, following a thorough investigation, 36 samples of landslides in the study area were chosen, and monitoring data spanning more than ten years revealed that most of the landslides had displacements of less than 800 mm and that all of them were in a stable (unstable) state with no overt indications of accelerated deformation. As a result, it was determined that the 31 landslides previously mentioned were in the creep stage. From the perspective of slope structure and morphology, the great majority of these landslides are downward slopes; the profile form is dominated by straight lines; and the slope height ratio is concentrated in a range of approximately 0.25. These characteristics suggest that these landslides are typically long and narrow, with a relatively gentle surface on the slope body, a small thickness, and easy penetration by rainfall. The cohesive force is primarily within 20 kPa, and the friction angle is primarily around 20°, suggesting that the landslides have the capacity to generate a greater anti-slip force.

To exclude rainfall events that do not induce significant displacement, a generalized geological model was established in GeoStudio for seepage-stress coupling analysis³⁶, based on statistical parameters of 31 creeping landslides in the study area (average length: 300 m, thickness: 20 m, slope angle: 15°, $c \approx 20$ kPa, $\phi \approx 20^\circ$). Using the accuracy of commercial GPS equipment ($\pm 1-2$ mm) as the lower limit for detectable displacement, the displacement responses under different rainfall amounts (10–50 mm) were simulated. The results show that when rainfall is < 30 mm, the displacement is < 1 mm and cannot be reliably monitored; when rainfall is ≥ 30 mm, the displacement response becomes significant. Therefore, 30 mm was set as the lower threshold for rainfall events to be included in the statistics, and rainfall processes below this value were excluded from the analysis.

Rainfall statistical variables

Three factors are often present in a rainstorm event: intensity, duration, and amount of rainfall. We chose rainfall volume and duration to identify rainfall events in the study region and utilized them to establish the statistical variables because it is not possible to acquire rainfall intensity with greater accuracy from the day-by-day rainfall data in the study area. The final rainfall statistical variables identified by time period are shown in Table 1 after combining the aforementioned three points and taking into account the factors that influence landslide movement in the reservoir area, the correlation between rainfall factors and landslide occurrence in the study area, and the response of landslide displacement to rainfall.

Selection of landslide deformation indicators

Traditional studies have predominantly used indicators such as absolute displacement values and displacement rates³⁷. However, these indicators are significantly influenced by landslide scale (length, thickness), making cross-regional comparisons difficult³⁸. Research indicates that the deformation of landslides in the creeping stage is directly related to landslide length, sliding mass thickness, and geotechnical parameters³⁹. To eliminate the scale effect, this study introduces the displacement ratio as a deformation indicator, defined as the ratio of cumulative displacement to landslide length. This indicator has a clear physical meaning, is easy to obtain, and is suitable for regional-scale rainfall warning modeling.

Reaction connection between rainfall statistics variables and displacement indicators

To address the mismatch in temporal scales between monthly displacement data and daily rainfall records⁴⁰, the following algorithm was employed to disaggregate monthly displacements into individual rainfall events:

- (1) Identify independent rainfall events within the month where cumulative rainfall ≥ 30 mm and there is at least one day without rainfall before and after the event.

Landslide	Location	Slow deformation stage displacement(mm)	Uniform deformation stage displacement(mm)	Landslide length(m)	Slow stage displacement ratio	Uniform stage displacement ratio
Xintan	Zigui	< 198	306–3060	2000	$< 9.9 \times 10^{-5}$	$(15.3-153.0) \times 10^{-5}$
JiMing Temple	Zigui	< 39.6	114–380	250	$< 15.8 \times 10^{-5}$	$(45.6-152.0) \times 10^{-5}$

Table 1. The ratio of displacement and length of typical landslides in different deformation phases. The displacement ratio of 10×10^{-5} , used as the characteristic value for warning threshold determination, is derived from the slow deformation stages of these typical landslides.

- (2) Let the total monthly displacement be D_m , and the cumulative rainfall for the i -th rainfall event in that month be R_i ; then the displacement induced by this rainfall event is $d_i = D_m \times \frac{R_i}{\sum_{j=1}^k R_j}$, where $\sum R_j$ is the cumulative rainfall of all independent rainfall events in the month.
- (3) For months without valid rainfall events, the displacement is attributed to other factors and is not included in the analysis.

Based on data from 35 GPS monitoring points, scatter plots of cumulative rainfall (x) versus displacement ratio (y) were established for each time period. By comparing the fitting effects of linear, power-law ($y = a \cdot x^b$), and exponential functions ($y = a \cdot e^{bx}$), it was found that the exponential function better captures the nonlinear characteristic of decelerating growth in displacement ratio as rainfall increases. The final functional relationship was determined as:

$$\begin{cases} \text{May} : y = 0.067 \cdot 10^{-5} e^{0.064x} (R^2 = 0.29) \\ \text{June, July, August} : y = 0.156 \cdot 10^{-5} e^{0.026x} (R^2 = 0.29) \\ \text{September} : y = 0.239 \cdot 10^{-5} e^{0.019x} (R^2 = 0.38) \end{cases} \quad (3)$$

The R^2 values ranged from 0.29 to 0.38, indicating that a single rainfall factor can explain approximately 30–40% of the displacement variation. This, on one hand, confirms that rainfall is a significant triggering factor for landslide deformation, and on the other hand, reflects the inherent complexity of the landslide system—where factors such as reservoir water level, lithology, and structural planes also play a role. For a single-factor model aimed at practical warning applications, this fitting accuracy is sufficient to meet the requirements for graded warning.

Establishing thresholds for rainfall

The characteristic value of the displacement ratio can be used to establish the corresponding rainfall threshold once the functional relationship equation between the rainfall statistical data and displacement index has been obtained. Since pile body slides account for the majority of landslides under professional surveillance in Zigui County, data from recent, comparable landslides are also gathered to determine the displacements of their slow deformation and isokinetic deformation stages, as indicated in Fig. 6 and Table 2. Upon summarization, the following conclusions can be drawn: if the landslide’s displacement ratio for a given period of time approaches 10×10^{-5} , it can be inferred that the movement of the landslide has momentarily entered the slow deformation or isochronous deformation period, and a warning is necessary. Equation (1) yields the appropriate rainfall thresholds of 78.3 mm, 160.1 mm, and 196.6 mm, respectively, based on this characteristic value. The results of the rainfall thresholds for the sample area indicated above can be applied to the entire research area because the landslides in the area are consistent with the natural environment and geological backdrop of the statistical sample. The conventional five-level warning zoning of creeping landslides at Zigui County was eventually achieved by combining the monitoring system with past landslide data in the area (Table 2). The warning idea in the previous section states that, for a given rainfall event, one should first assess the duration of the event and calculate the value of n (May $n=4$; June–August $n=5$; September $n=4$); next, one should compute the maximum value of the cumulative rainfall in the event for n consecutive days; and lastly, one should compare

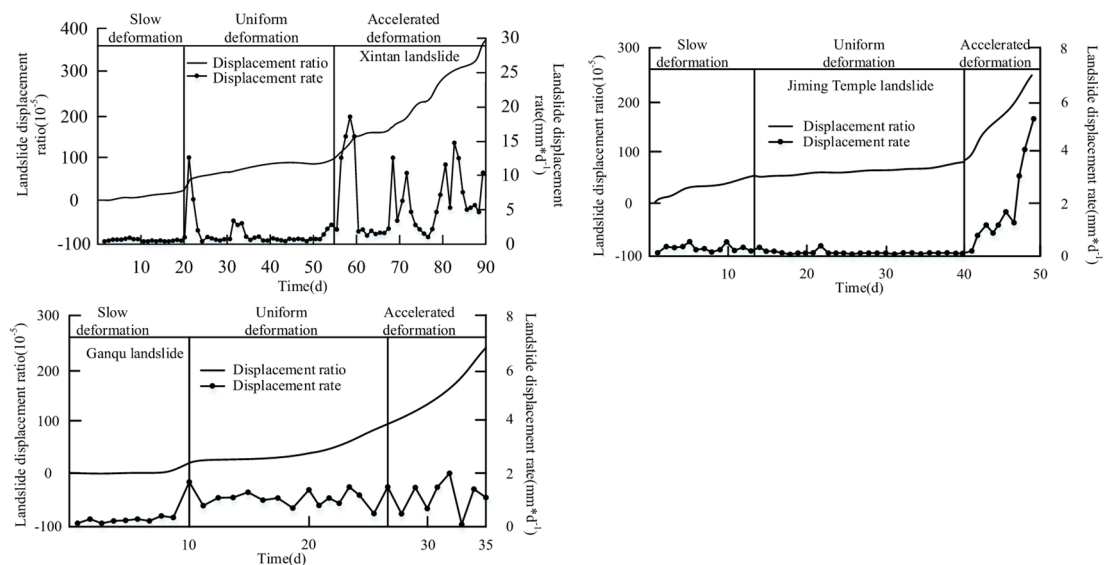


Fig. 6. The laws of ratio of displacement and length of some landslides.

Warning level	Stage of deformation	Disaster occurrence situation	Defense measures	Continuous rainfall for n days(mm)
1–2	Basically no deformation or minimal deformation	Small possibility	Not taking measures or paying attention to the monitoring of disaster points	0–78.3
3	Slow deformation	Medium possibility	Initiate group measurement and prevention work at disaster risk points, reminding people in the disaster area to pay attention to the dynamics of the disaster	78.3–160.1
4	Constant velocity deformation or brief acceleration deformation	Greater possibility	Strengthen monitoring of disaster points and implement preventive emergency measures for disaster risk areas	160.1–196.6
5	Accelerate deformation to failure	Maximum possibility	Monitor hidden danger points, organize emergency evacuation routes and disaster relief systems	> 196.6

Table 2. The warning levels of creeping landslide in Zigui County.

the maximum value with each rainfall threshold in Table 2 to determine the warning level in which the event is located and to take the appropriate action.

To account for the uncertainty in the statistical relationship between rainfall and the displacement ratio, a bootstrap resampling method was employed to estimate the 90% confidence intervals for the rainfall thresholds. For each period (May, June–August, and September), the original displacement–rainfall data pairs were randomly resampled with replacement (1000 iterations), and a power function model $y = a \cdot x^b$ was refitted for each bootstrap sample. Based on each fitted model, the rainfall amount corresponding to the characteristic displacement ratio value of 10×10^{-5} was calculated. The 2.5th and 97.5th percentiles of the 1000 bootstrap estimates were taken as the lower and upper bounds of the 90% confidence interval, respectively.

Results and analysis

Real-time rainfall data, landslide deformation monitoring data, and historical extreme rainfall events in the study area during 2016 were selected to carry out early warning forecasts of landslides, respectively, for the established rainfall early warning model for landslides in Zigui County. The final results were compared with the actual situation to check the early warning capability of the model. With the exception of a few landslides that have entered or are about to enter the state of near-slip, all potential landslide sites in the area are in the creep period, according to data from Zigui County's monitoring station. As a result, the model developed for this study can be used to conduct rainfall early warning systems. Based on statistical data, there were three larger-scale (> 150 m³) landslide threats in the area during the 2021 flood season:

- (1) On June 9, 2021, a hazardous scenario with a 150,000 m³ volume occurred on a slope in Guojiaba Township. The disaster management department initially evacuated six residents of the slope because it was not an original group monitoring and prevention point. Once the incident was handled, a new group monitoring and prevention point was established in the neighborhood to track the dynamics of the landslide's development;
- (2) On June 27, 2021, after intense rain, there was a brief period of sluggish slope displacement at Shuitianba, resulting in a 120 × 150 m³ landslide. The locals were cautioned by the authorities to keep a close check on the dynamics of the landslide, as it was eventually stopped with minimal damage to the houses and no casualties. This point has been included in the group monitoring and prevention monitoring points;
- (3) On August 28, 2021, three residential homes were damaged in Guizhou Township, when a 40,000 m³ landslide threat occurred. Thankfully, all villagers in danger were evacuated ahead of schedule and without any casualties as a result of the early warning system, monitoring, and prompt emergency response. Following the incident, a new group monitoring and defense point was established in the area to track the landslide's progress.

Since all of the above risky circumstances happened between June and August, $n=5$. The values of the rainfall statistical variables in the 20 days before and after the occurrence of the three dangerous situations were further calculated, along with their corresponding model warning levels. The results are shown where the value of The “total rainfall for 5 consecutive days” is the sum of the rainfall for the 5 days prior to that day. The cumulative rainfall changes in the previous 5 days when the dangerous situations occurred were calculated, and the results are shown in Table 3. From Table 3, it was found that the model prediction results coincided with the actual countermeasures taken. The warning level for that day represented by the red warning line in the illustration, which graphically depicts the warning level at which the landslide is placed on that particular day can be ascertained by comparing this value with each rainfall threshold in Table 3. The Fig. 7 shows that the day of all landslides has the highest warning level during the time period (the red warning line is equal to or higher than the other times), and that the warning level one to three days prior to and following the occurrence of the danger is lower. This suggests that the model's warning is more timely, demonstrating its viability, and that the prediction result is more accurate.

Comprehensive monitoring data for the creeping landslides in Zigui County are available, and their displacement–time curves can be used to both visualize the movement characteristics of landslides during periods of rainfall and serve as a foundation for early warning systems for landslides. In the research area, three GPS monitoring sites on various landslides were chosen, and each of them exhibited “step” displacement–time curves that were comparable to one another (Fig. 8). Every step period's rainfall variables and landslide displacement indicators were statistically analyzed to determine the model's warning outcomes. The results

Time of occurrence of dangerous situation	Location	Rainfall variable values(mm)	Model warning results	Measures to be taken at this level	Actual disposal situation
09/06/2021	Guojiaba town	13.36	Level 2 warning	Paying attention to the monitoring of disaster points	Group monitoring and prevention points have been established to remind residents to pay close attention to monitoring data and macroscopic deformation
27/06/2021	Shuitian dam	66.98	Level 3 warning	Initiate group measurement and prevention work at disaster risk points, reminding people in the disaster area to pay attention to the dynamics of the disaster	Emergency evacuation of residents and subsequent initiation of mass testing and prevention work at the site
28/08/2021	Guizhou town	53.39	Level 3 warning	Same as above	Initiated group testing and defense work for this point

Table 3. The statistical information of Zigui County landslides in the year of 2021.

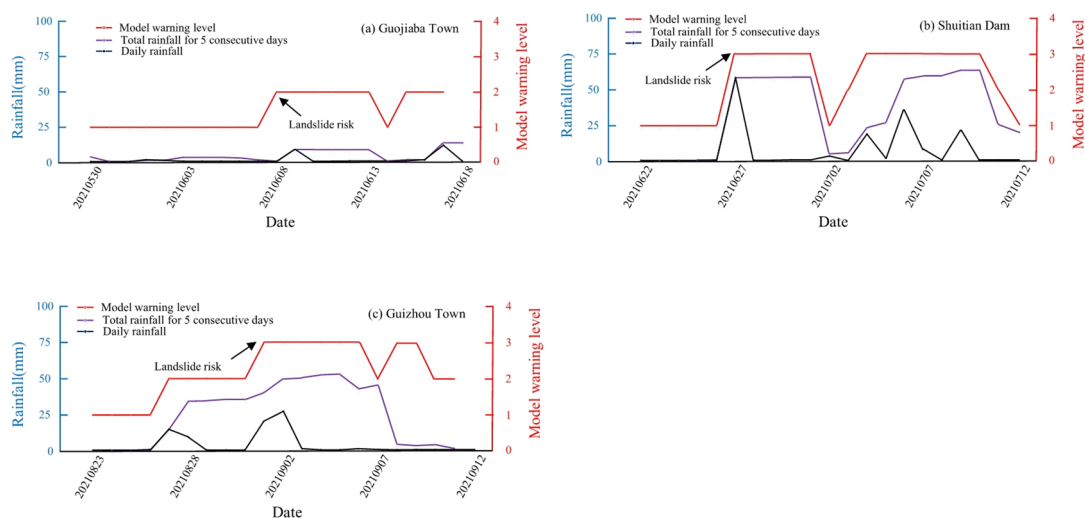


Fig. 7. The comparison between model warning results and actual situations of landslide cases in 2021.

showed that during each time of sharply increasing displacement, there were at least two, and occasionally even four, warnings. The “step periods” in which each landslide’s maximum displacement increment occurred were counted using the displacement data of all 28 landslides in order to identify a more general pattern. Each “step period” corresponded to at least two warning levels, and the majority of the corresponding displacement ratio indicators were near or in most circumstances, the ratio of the displacement value during this period to the overall displacement of the monitoring point can approach 20% or even 40%. The corresponding displacement ratio indicators are generally near or above the characteristic value of 10×10^{-5} indicated above; and the relevant units’ monitoring report demonstrates that the abrupt shift in the landslide’s displacement in the real situation has resulted in varying degrees of economic losses, such as home damage. In response, appropriate steps have been taken to lower the risk of landslides by evacuating pertinent personnel and bolstering the data collection process. The accuracy of the model is demonstrated by the warning findings from the landslide GPS monitoring locations matching the real scenario.

Due to the concentration of rainfall in the study area during the flood season, several extreme rainfall events have occurred historically. According to the model of this study, the cumulative rainfall in the early part of the event was greater than the rainfall threshold of 196.6 mm, which required emergency evacuation of residents to avoid landslide risks. The actual situation shows that this rainfall process caused 394 landslides and 240 dangerous landslides in two days, resulting in significant casualties and economic losses, which also verifies the accuracy and reliability of the model’s warning results.

Quantitative validation using 2021 events

To quantitatively evaluate the warning model’s predictive performance, we constructed a contingency table (confusion matrix) for the 2021 flood season (May 1 to September 30). A warning was considered “positive” if the model output reached Level 3 or higher (i.e., cumulative rainfall exceeded the slow deformation threshold). Actual landslide occurrences were defined as the three hazardous events documented in Sect. “Results and analysis” (June 9, June 27, and August 28). The resulting confusion matrix is shown in Table 4.

The model successfully detected all three hazardous events (no false negatives), indicating high sensitivity (recall = 100%). However, it also issued 12 false alarms (warnings without actual landslides), resulting in a relatively low precision (20%). This means that only one out of every five warnings correctly predicted an event.

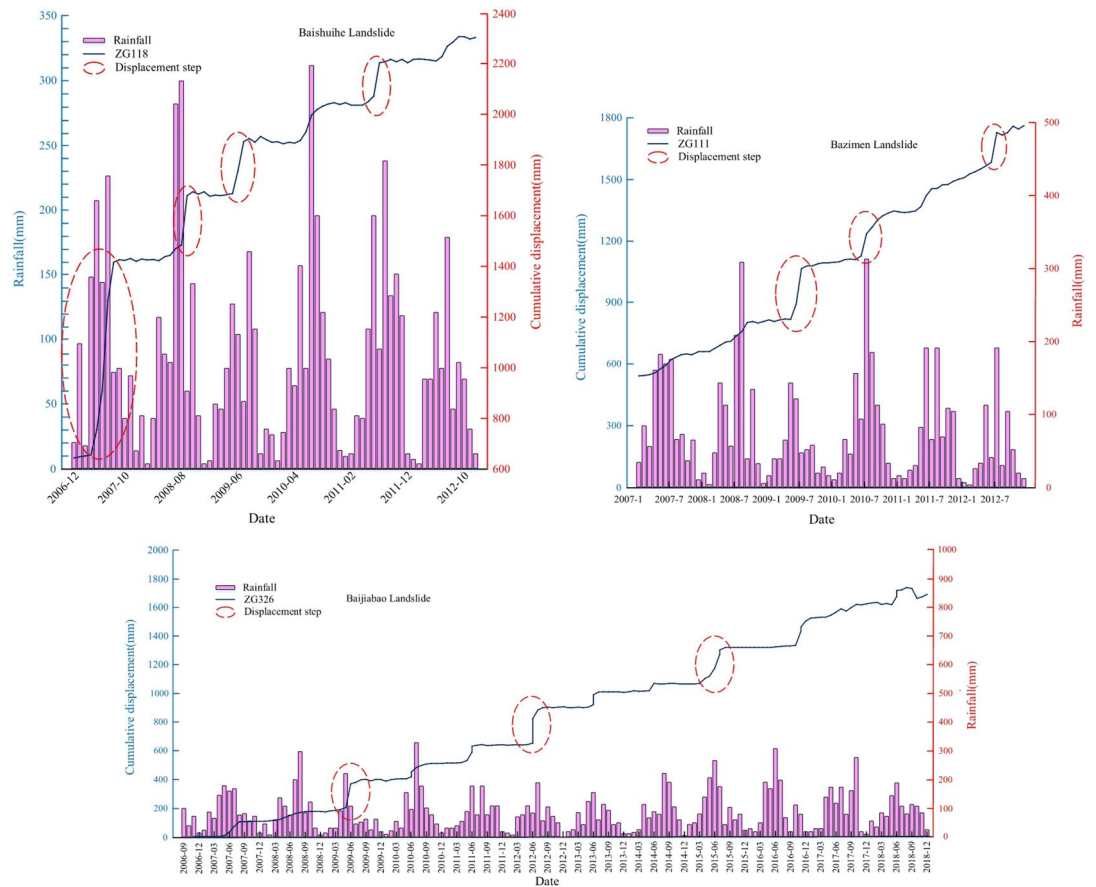


Fig. 8. The step-like displacement curve of creeping landslide in Zigui County.

	Actual landslide (yes)	Actual landslide (no)
Warning \geq level 3	TP = 3	FP = 12
Warning \leq level 2	FN = 0	TN = 138

Table 4. Confusion matrix for the 2021 warning performance. From this matrix, we derived the following performance metrics: True positive rate (Recall) = $3/(3 + 0) = 1.00$, False positive rate = $12/(12 + 138) = 0.08$, Precision = $3/(3 + 12) = 0.20$, Accuracy = $(3 + 138)/153 = 0.92$, F1-score = $2 \times (0.20 \times 1.00)/(0.20 + 1.00) = 0.33$.

The false positive rate of 8% suggests that the model tends to be conservative, which is acceptable for early warning systems prioritizing safety, but could lead to warning fatigue if not managed properly. The high accuracy (92%) is largely driven by the numerous true negatives (days with no warning and no landslide). Overall, the model demonstrates strong capability in capturing actual landslide events, albeit at the cost of some false alarms.

Retrospective analysis of a historical extreme rainfall event

To further assess the model's performance under extreme conditions, we applied it to a historical heavy rainfall event that occurred in the study area. During this event, the cumulative rainfall exceeded the Level 5 warning threshold of 196.6 mm established by the model. According to historical records, this rainfall process triggered 394 landslides and 240 hazardous situations over two days, resulting in significant casualties and economic losses.

Applying the model to this event, the cumulative rainfall for n consecutive days ($n = 5$ for the June–August period), corresponding to a Level 5 warning. This indicates that the model would have issued the highest level of alert prior to the event, recommending emergency evacuation of residents. The actual consequences confirm the severity of the event and demonstrate that the model's highest warning level accurately captured the risk. This retrospective analysis, although based on a single historical event, provides additional evidence of the model's capability to identify extreme rainfall conditions that lead to widespread landslide occurrences. It complements the 2021 validation by testing the model against a different type of rainfall event with catastrophic outcomes.

Discussion

The rainfall early warning model is mainly based on historical cases with records of rainfall history and landslide-related information, and establishes a relationship model between landslides and rainfall by statistically analyzing the effects of rainfall duration, rainfall amount, intensity and rainfall type on landslides. The Three Gorges Reservoir area is rich in rainfall data, but it is a vast area, and the rainfall and geomorphological conditions in a large spatial area are complex and diverse, and the rainfall type landslides are affected by rainfall conditions, slope topography and geological conditions, and it is difficult to fully quantify and analyze the rainfall warning thresholds. For the rainfall threshold model of landslides in large space area, combined with the characteristics of rainfall-type landslides, historical rainfall conditions, etc., it can be refined regional division, such as damage mode, slope structure, slope morphology, and systematically carry out the refined warning threshold analysis of landslides with different development characteristics, which can better warn rainfall-type landslides in the region, and no longer confined to the regional macroscopic rainfall thresholds for early warning.

Although the rainfall early warning model developed in this study has demonstrated considerable effectiveness in predicting creep-type landslides in Zigui County, several limitations remain:

- (1) *Limited explanatory capacity*: Statistical analysis indicates that the model accounts for only about 30–40% of the variance in the landslide displacement ratio. While rainfall serves as a significant triggering factor, landslide deformation is also influenced by multiple interacting factors, including reservoir water level fluctuations, geomechanical properties of rock and soil masses, and geological structure.
- (2) *Dependence on high-density professional monitoring*: Both the development and validation of the model rely on data from densely deployed GPS monitoring stations within the study area. Such monitoring networks may be difficult to replicate in other regions, thereby constraining the model's direct transferability.
- (3) *Lack of external validation*: Validation of the model has been confined to Zigui County; its performance has not been tested in regions with differing geological or climatic conditions. Consequently, the generalizability of the model remains uncertain.

Future research should integrate multi-source data (e.g., InSAR, rainfall forecasts, hydrological monitoring) to explore multi-factor coupled early warning models. Validation efforts should also be extended to broader geographic contexts to enhance the model's applicability and robustness.

Conclusion

This study focused on creeping landslides in Zigui County within the Three Gorges Reservoir area and proposed a rainfall warning method based on a displacement ratio model. The main conclusions are as follows:

- (1) The displacement ratio (displacement/landslide length) was introduced as a deformation indicator, effectively eliminating the influence of landslide scale and endowing the model with potential for cross-regional comparison.
- (2) Based on correlation analysis and numerical simulation, cumulative rainfall was identified as the core warning variable, and time-phased exponential response models were established for different periods (May, June–August, and September). The models explain approximately 30–40% of the displacement variation, reflecting the contribution of rainfall as the main controlling factor.
- (3) Four-level warning thresholds (78.3 mm, 160.1 mm, and 196.6 mm) were determined, establishing a five-level warning system. Validation using three landslide events in 2021 showed that the model successfully issued warnings for all incidents (100% recall), albeit with an 8% false alarm rate, indicating that the model is conservative yet practically valuable.
- (4) The model relies on high-density GPS monitoring data and has only been validated in this region; its extrapolation to other areas requires adaptive modifications based on local geological conditions. Future research should incorporate multi-source data and explore multi-factor coupled warning models to improve prediction accuracy and generalization capability.

Data availability

The landslide displacement data used in this study were obtained from the professional monitoring network operated by the Department of Natural Resources of Hubei Province and the Geological Environment Monitoring Station of Zigui County. These data are classified as sensitive geological information under Chinese regulations and cannot be publicly shared due to national security and confidentiality agreements with the local authorities. The rainfall data used in this study are publicly available from the China Meteorological Data Service Centre upon registration. Metadata, including the time series of displacement measurements (without precise coordinates), the statistical summaries of landslide characteristics (length, thickness, slope angle), and the derived displacement ratios, are available from the corresponding author upon reasonable request and with permission from the data owner. Researchers interested in accessing the underlying data may contact the corresponding author (xyin0320@163.com) to discuss collaboration opportunities or to request access through official channels with the approval of the Hubei Provincial Department of Natural Resources.

Received: 4 September 2025; Accepted: 27 February 2026

Published online: 08 March 2026

References

1. Haque, U. et al. The human cost of global warming: Deadly landslides and their triggers (1995–2014). *Sci. Total Environ.* **682**, 673–684 (2019).

2. Zhang, K. et al. Characteristics and influencing factors of rainfall-induced landslide and debris flow hazards in Shaanxi Province, China. *Nat. Hazards Earth Syst. Sci.* **19**(1), 93–105 (2019).
3. Wang, Z. et al. Regional landslide hazard assessment through integrating susceptibility index and rainfall process. *Nat. Hazards* **104**(3), 2153–2173 (2020).
4. Pecoraro, G., Calvello, M. & Piciullo, L. Monitoring strategies for local landslide early warning systems. *Landslides* **16**, 213–231 (2019).
5. Yang, Z. et al. Application and verification of a multivariate real-time early warning method for rainfall-induced landslides: Implication for evolution of landslide-generated debris flows. *Landslides* **17**, 2409–2419 (2020).
6. Thirugnanam, H., Ramesh, M. V. & Rangan, V. P. Enhancing the reliability of landslide early warning systems by machine learning. *Landslides* **17**(9), 2231–2246 (2020).
7. Meng, W. et al. Phase-field modeling of cracking process in partially saturated porous media and application to rainfall-induced landslides. *Eng. Geol.* **310**, 106884 (2022).
8. Feng, R. et al. Two-phase fully-coupled smoothed particle hydrodynamics (SPH) model for unsaturated soils and its application to rainfall-induced slope collapse. *Comput. Geotech.* **151**, 104964 (2022).
9. Lee, J. H. et al. Temporal prediction modeling for rainfall-induced shallow landslide hazards using extreme value distribution. *Landslides* **18**, 321–338 (2021).
10. Lin, Q. et al. Assessing the spatiotemporal impact of climate change on event rainfall characteristics influencing landslide occurrences based on multiple GCM projections in China. *Clim. Change* **162**, 761–779 (2020).
11. Zhao, B. et al. Assessing the potential of different satellite soil moisture products in landslide hazard assessment. *Remote Sens. Environ.* **264**, 112583 (2021).
12. Xue, C. et al. Heavy rainfall drives slow-moving landslide in Mazhe village, Enshi to a catastrophic collapse on 21 July 2020. *Landslides* <https://doi.org/10.1007/s10346-021-01782-7> (2022).
13. Wu, K. et al. Failure mechanism of the Yaoba loess landslide on March 5, 2020: The early-spring dry spell in Southwest China. *Landslides* **18**, 3183–3195 (2021).
14. Park, H. J., Jang, J. Y. & Lee, J. H. Assessment of rainfall-induced landslide susceptibility at the regional scale using a physically based model and fuzzy-based Monte Carlo simulation. *Landslides* **16**, 695–713 (2019).
15. Pelascini, L. et al. Finite-hillslope analysis of landslides triggered by excess pore water pressure: The roles of atmospheric pressure and rainfall infiltration during typhoons. *Nat. Hazards Earth Syst. Sci.* **22**(10), 3125–3141 (2022).
16. Yang, B. et al. Time series analysis and long short-term memory neural network to predict landslide displacement. *Landslides* **16**, 677–694 (2019).
17. Zhang, Y. et al. Forecasting the magnitude of potential landslides based on InSAR techniques. *Remote Sens. Environ.* **241**, 111738 (2020).
18. Zhang, J. et al. Deformation stage division and early warning of landslides based on the statistical characteristics of landslide kinematic features. *Landslides* <https://doi.org/10.1007/s10346-023-02192-7> (2024).
19. Xu, Q. et al. Successful implementations of a real-time and intelligent early warning system for loess landslides on the Heifangtai terrace, China. *Eng. Geol.* **278**, 105817 (2020).
20. Scoppettuolo, M. R., Cascini, L. & Babilio, E. Typical displacement behaviours of slope movements. *Landslides* **17**(5), 1105–1116 (2020).
21. Tanyaş, H. et al. Rapid prediction of the magnitude scale of landslide events triggered by an earthquake. *Landslides* **16**, 661–676 (2019).
22. Nava, L. et al. Landslide displacement forecasting using deep learning and monitoring data across selected sites. *Landslides* **20**(10), 2111–2129 (2023).
23. Hua, Y. et al. Dynamic development of landslide susceptibility based on slope unit and deep neural networks. *Landslides* **18**, 281–302 (2021).
24. Pan, Y. & Zhang, L. Integrating BIM and AI for smart construction management: Current status and future directions. *Arch. Comput. Methods Eng.* **30**(2), 1081–1110 (2023).
25. Close, M. E., Humphries, B. & Northcott, G. Outcomes of the first combined national survey of pesticides and emerging organic contaminants (EOCs) in groundwater in New Zealand 2018. *Sci. Total Environ.* **754**, 142005 (2021).
26. Dai, Z. et al. Interpreting the influence of rainfall and reservoir water level on a large-scale expansive soil landslide in the Danjiangkou Reservoir region, China. *Eng. Geol.* **288**, 106110 (2021).
27. Yan, L. et al. Drainage controls on the Donglingxing landslide (China) induced by rainfall and fluctuation in reservoir water levels. *Landslides* **16**, 1583–1593 (2019).
28. Li, C. et al. Susceptibility of reservoir-induced landslides and strategies for increasing the slope stability in the Three Gorges Reservoir Area: Zigui Basin as an example. *Eng. Geol.* **261**, 105279 (2019).
29. Hou, T. S. et al. Stability analysis of Gongjiacun landslide in the three Gorges reservoir area under the action of reservoir water level fluctuation and rainfall. *Nat. Hazards* **114**(2), 1647–1683 (2022).
30. Yin, H. et al. Predicting mine water inrush accidents based on water level anomalies of borehole groups using long short-term memory and isolation forest. *J. Hydrol.* **616**, 128813 (2023).
31. Bai, N. et al. Graded intrafillable architecture-based iontronic pressure sensor with ultra-broad-range high sensitivity. *Nat. Commun.* **11**(1), 209 (2020).
32. Uwihirwe, J., Hrachowitz, M. & Bogaard, T. A. Landslide precipitation thresholds in Rwanda. *Landslides* **17**(10), 2469–2481 (2020).
33. Rengers, F. K. et al. Landslides after wildfire: Initiation, magnitude, and mobility. *Landslides* **17**(11), 2631–2641 (2020).
34. Valenzuela, P. et al. Empirical rainfall thresholds for the triggering of landslides in Asturias (NW Spain). *Landslides* **16**, 1285–1300 (2019).
35. Picarelli, L. et al. The effects of extreme precipitations on landslide hazard in the pyroclastic deposits of Campania region: A review. *Landslides* **17**(10), 2343–2358 (2020).
36. Palau, R. M. et al. Application of a fuzzy verification framework for the evaluation of a regional-scale landslide early warning system during the January 2020 Gloria storm in Catalonia (NE Spain). *Landslides* **19**(7), 1599–1616 (2022).
37. Chen, M., Huang, D. & Jiang, Q. Slope movement classification and new insights into failure prediction based on landslide deformation evolution. *Int. J. Rock Mech. Min. Sci.* **141**, 104733 (2021).
38. Liu, Y. et al. Landslide displacement prediction based on multi-source data fusion and sensitivity states. *Eng. Geol.* **271**, 105608 (2020).
39. Zhan, J. et al. Soil-engineering properties and failure mechanisms of shallow landslides in soft-rock materials. *CATENA* **181**, 104093 (2019).
40. Xue, Y. et al. Dynamic stability assessment of reservoir colluvial landslide using a hypoplastic clay constitutive model considering the effects of drying-wetting cycles on the hydro-fluctuation belt. *Eng. Geol.* **307**, 106791 (2022).

Acknowledgements

We would highly thank the Department of surveying and mapping of Hubei Province for providing relevant data.

Author contributions

Yin Xing: Writing—original draft, Funding acquisition. Saipeng Huang: Supervision. Peng Wang: Project administration, Investigation, Data curation.

Funding

This research was funded by the CRSRI Open Research Program (Program SN: CKWV20241187/KY); Key Laboratory of Land Satellite Remote Sensing Application, Ministry of Natural Resources of the People's Republic of China (KLSMNR-G202304); Key Laboratory of Coastal Salt Marsh Ecosystems and Resources, Ministry of Natural Resources (KLCSMERMNR202306); The Natural Science Foundation of the Jiangsu Higher Education Institutions of China (25KJB420006); Vice President of Science and Technology of Jiangsu Province (FZ20251106); Jiangsu Provincial Engineering Center for Industrial Technology of Urban Intelligent Remote Sensing and Ancient City Digital Intelligence.

Declarations

Competing interests

The authors declare no competing interests.

Additional information

Correspondence and requests for materials should be addressed to Y.X.

Reprints and permissions information is available at www.nature.com/reprints.

Publisher's note Springer Nature remains neutral with regard to jurisdictional claims in published maps and institutional affiliations.

Open Access This article is licensed under a Creative Commons Attribution-NonCommercial-NoDerivatives 4.0 International License, which permits any non-commercial use, sharing, distribution and reproduction in any medium or format, as long as you give appropriate credit to the original author(s) and the source, provide a link to the Creative Commons licence, and indicate if you modified the licensed material. You do not have permission under this licence to share adapted material derived from this article or parts of it. The images or other third party material in this article are included in the article's Creative Commons licence, unless indicated otherwise in a credit line to the material. If material is not included in the article's Creative Commons licence and your intended use is not permitted by statutory regulation or exceeds the permitted use, you will need to obtain permission directly from the copyright holder. To view a copy of this licence, visit <http://creativecommons.org/licenses/by-nc-nd/4.0/>.

© The Author(s) 2026